Journal of Power Sources 465 (2020) 228264

Contents lists available at ScienceDirect

Journal of Power Sources

journal homepage: www.elsevier.com/locate/jpowsour

Simultaneously enhancing power density and coulombic efficiency with a hydrophobic Fe–N_4/activated carbon air cathode for microbial fuel cells

Wulin Yang [a], Xu Wang [b], Moon Son [a], Bruce E. Logan [a,*]

[a] Department of Civil and Environmental Engineering, The Pennsylvania State University, University Park, PA, 16802, United States
[b] School of Resource and Environmental Sciences, Hubei International Scientific and Technological Cooperation Base of Sustainable Resource and Energy, Wuhan University, No. 129 Luoyu Road, Wuhan, 430079, PR China

HIGHLIGHTS

- A hydrophobic Fe–N_4/AC composite investigated as cathode catalyst for MFCs.
- MFCs with 10 wt% Fe–N_4/AC cathodes showed a 25% increase in power performance.
- The hydrophobic Fe–N_4/AC catalyst reduced water electrolyte evaporation.
- Coulombic efficiency was simultaneously increased for the 10 wt% Fe–N_4/AC cathodes.

ARTICLE INFO

Keywords:
Hydrophobicity
Fe–N_4 macromolecule
Oxygen reduction
Activated carbon air cathode
Microbial fuel cell

ABSTRACT

The application of microbial fuel cells (MFCs) for electricity generation is still hindered by relatively low power densities and coulombic efficiencies. Here a hydrophobic Fe–N_4 macromolecule catalyst was directly immobilized on the activated carbon (AC) surface to fabricate a hydrophobic Fe–N_4/AC air cathode. With a 10 wt% Fe–N_4/AC cathode, a maximum power density of 2.5 ± 0.1 W m^{-2} was obtained, which was 25% higher than plain AC cathodes (2.0 ± 0.01 W m^{-2}). The additional hydrophobicity due to the Fe–N_4 macromolecule catalyst simultaneously reduced water electrolyte evaporation and oxygen intrusion for improved coulombic efficiency. The coulombic efficiency was increased to 20 ± 0.5% for the 10 wt% Fe–N_4/AC cathode, which was ~54% higher than that of the AC cathodes (13 ± 0.2%) at an external resistance of 1000 Ω. The use of hydrophobic Fe–N_4 macromolecule catalyst is the first attempt to simultaneously improve the power density and coulombic efficiency by tuning the catalyst hydrophobicity, which also explores a new direction of catalyst engineering for the advancement of MFCs.

1. Introduction

Microbial fuel cell (MFC) is a sustainable technology to harvest electric energy from wastewater, achieving a green wastewater treatment plant with minimum energy consumption [1–6]. In an MFC the exoelectrogenic bacteria on the anode degrade organics in the wastewater and release electrons to the cathode via an external circuit [7–9]. The oxygen reduction reaction (ORR) usually is used at the cathode due to the abundance of oxygen in atmosphere [10–14]. Activated carbon (AC) is currently the mostly widely used oxygen reduction catalyst in an air cathode due to its low cost of $1.4 kg^{-1} compared to platinum ($625 g^{-1}) [15–17]. While AC is economically preferable to Pt, the sluggish ORR kinetics have contributed to low power production, hindering wider applications of MFCs [2,18,19]. Moreover, AC contains hydroxyl or carboxyl groups that increase the hydrophilicity of air cathodes, which leads to fast water evaporation at the water/air interphase. The water loss enables greater air intrusion into the reactor fluid, lowering the coulombic efficiency as well as energy recovery in the MFCs [10].

Heteroatom doping and co-catalyst immobilization are currently the two main methods being explored to improve the catalytic activity of AC. Heteroatoms such as nitrogen, sulfur, and phosphorus, can be doped into the carbon matrix of AC to introduce more catalytic sites [20–22]. Nitrogen doping was reported to be most effective among these elements due to the formation of pyridinic nitrogen functional groups as effective catalytic sites for the ORR [23]. However, the doping efficiency is usually low and this leads to a high level of precursor materials

* Corresponding author.
E-mail address: blogan@psu.edu (B.E. Logan).

https://doi.org/10.1016/j.jpowsour.2020.228264
Received 25 February 2020; Received in revised form 16 April 2020; Accepted 25 April 2020

consumption. For example, five times as much mass of cyanamide was used added to AC to obtain a 5% pyridinic nitrogen doping, making this a relatively expensive approach for improved performance [24]. The second method of co-catalyst immobilization has reduced the use of precursor materials by directly immobilizing a more reactive ORR catalyst on the AC surface. Among different types of co-catalysts such as transitional metal oxides and precious metals, iron–nitrogen-carbon (Fe–N–C) co-catalyst is most appealing due to its high catalytic activity and low material cost [25,26]. A Fe–N–C/AC composite catalyst was synthesized by carbonizing iron chloride and 1,10–phenanthroline with AC at 800 °C, consuming only one sixth in mass of AC of the precursors and producing the highest power density of 2.6 W m^{-2} in MFCs in the literature under otherwise similar test conditions [27]. Although Fe–N–C co–catalyst has shown great promise in terms of high performance and low material consumption, the need for a high temperature synthesis procedure could hinder mass production for larger scale applications. Moreover, these Fe–N–C/AC composite catalysts were typically pyrolyzed and lost their original functional groups for hydrophobicity/hydrophilicity tuning, which had little impact on the water/air interphase, and thus could not aid in improving coulombic efficiency.

Enhancing the hydrophobicity of air cathodes seems a straightforward strategy to reduce water evaporation and increase the coulombic efficiency. More conventional ways of tuning hydrophobicity of air cathodes is through addition of hydrophobic polymer binders. For example, a hydrophobic poly(dimethyl siloxane) (PDMS) polymer was used in AC catalyst layer to avoid water intrusion (flooding of catalyst) for a more efficient water/air catalytic interface, with higher power production than using hydrophilic Nafion binders over 15 days of operation [28]. Other hydrophobic polymer binders such as polyvinylidene fluoride and polytetrafluoroethylene have also been recently used to fabricate AC air cathodes [15,29,30]. However, the added amount of hydrophobic binders must be limited as their addition leads to increased electrical impedance and ion diffusion hindrance resulting in decreased performance. Alternative methods of tuning the hydrophobicity of air cathodes is needed to avoid the negative impact on power production. Using a hydrophobic co–catalyst instead to tune the hydrophobicity of AC air cathodes could be a more promising route but has not been previously investigated.

Iron phthalocyanine, a macrocyclic complex, has long been adopted as a co-catalyst towards ORR in fuel cell, battery, and MFC fields. The capability of iron phthalocyanine to facilitate ORR was first observed in a fuel cell in 1964 [31]. Since then, iron phthalocyanine has been immobilized on different substrates such as carbon nanotubes, carbon black, and graphene, to improve the performance of ORR catalysts [32–35]. The previous studies mainly focused on the improvement of power production, but coulombic efficiency is also important for energy recovery. The hydrophobic properties of iron phthalocyanine have not been previously explored in MFCs for enhancing coulombic efficiencies.

In this study, the hydrophobic catalyst of iron phthalocyanine with a Fe–N_4 catalytic center, was directly immobilized on AC surface to form a hydrophobic Fe–N_4/AC composite catalyst for the air cathodes in MFCs. The hydrophobic nature of Fe–N_4/AC composite catalyst was examined in terms of its impact on both power production and coulombic efficiency in MFCs. The change in the hydrophobicity of air cathodes with different Fe–N_4 loadings was evaluated by dynamic contact angle measurements. The surface morphology and distribution of Fe–N_4/AC catalyst were characterized with scanning electron microscopy (SEM) and energy dispersive X-Ray spectroscopy (EDS). The catalytic performance of the Fe–N_4/AC cathodes was tested in both the MFC reactors and abiotic electrochemical cells.

2. Material and methods

2.1. Preparation of Fe–N_4/AC cathodes

To fabricate the Fe–N_4/AC composite catalysts, different amounts of iron phthalocyanine (Alfa Aesar, USA) was firstly dispersed in 100 mL of ethanol, and stirred at 60 °C for 2 h in a capped bottle to prevent ethanol evaporation. AC powder (Norit SX plus, Norit Americas Inc., TX) was then added into the iron phthalocyanine/ethanol solution with mass percentage of iron phthalocyanine: AC = 0.1, 1.0 and 10 wt%. The slurry was further stirred at 60 °C until dry due to ethanol evaporation. The Fe–N_4/AC catalysts were then further dried in a vacuum oven at 80 °C for 12 h. The control AC catalyst was treated with the same method but without any iron phthalocyanine addition.

The air cathodes were prepared using a hot pressing method as previously described [16,36]. Briefly, 6 g of the Fe–N_4/AC or plain AC catalyst was dispersed in deionized water and stirred on a hot plate at 60 °C. A 60% PTFE (polytetrafluoroethylene) emulsion was then added into the slurry at a mass ratio of 6:1 (Catalyst: PTFE). The mixture was continuously stirred and heated with water evaporating to form a gel. The gel was then pressed at 1×10^7 Pa for 2 s at 60 °C with a pressing machine (Model 4388, CARVER, INC., USA), and folded and pressed again two more times. The prepared catalyst layer had a catalyst (Fe–N_4/AC or plain AC) loading of 27 ± 1 mg cm^{-2}. This catalyst layer was then placed between a stainless steel mesh current collector (42 × 42, type 304, McMaster-Carr, USA) and a hydrophobic PVDF membrane diffusion layer (0.45 μm, MILLIPORE, USA). The final structure was then rinsed with ethanol, pressed together at 3×10^7 Pa for 15 s at 60 °C, and then dried in a fume hood at room temperature.

2.2. MFC construction and operation

Single chamber MFCs were constructed from a Lexan block with a cylindrical chamber 4 cm long and 3 cm in diameter [37,38]. The graphite fiber brush anodes (2.5 cm in both diameter and length) were heat treated at 450 °C in air for 30 min prior to use. The anodes were placed horizontally in the middle of MFC chambers, with 1 cm distance between the brush tip and the cathode. The anodes had been acclimated and operated in batch mode in MFCs for over one year, in a constant temperature room (30 °C). The medium were 1 g L^{-1} sodium acetate dissolved in a 50 mM phosphate buffer solution (PBS) (Na_2HPO_4, 4.58 g L^{-1}; $NaH_2PO_4{\cdot}H_2O$, 2.45 g L^{-1}; NH_4Cl, 0.31 g L^{-1}; KCl, 0.13 g L^{-1}; pH = 6.9; κ = 6.94 mS cm^{-1}) amended with 12.5 mL L^{-1} minerals and 5 mL L^{-1} vitamins [39].

The power performance of MFCs was characterized using a single cycle polarization method as previously described [37], by varying the external resistance from 1000, 500, 200, 100, 75, 50 to 20 Ω at 20 min intervals after initial operation with an open circuit for 2 h. The reactors were operated for two cycles prior to the polarization test to stabilize the cathodes, with one cycle of one day. All polarization tests were conducted in duplicate in a constant temperature room at 30 °C, and the mean values were reported for the power density. Voltage drop (U) across an external resistor was recorded by a data acquisition system (2700, Keithley Instrument, OH). Current densities (i) and power densities (P) were calculated as $i = U/RA$ and $P = iU/A$ (R is the external resistance), and normalized to the cathode projection area ($A = 7$ cm^2). The measured anode potentials ($E_{An,m}$) were calculated from the potential difference between anode and an Ag/AgCl reference electrode (RE-5B, BASi, West Lafayette, IN; + 0.209 V vs a standard hydrogen electrode) that was placed close to the anode brush. The anode potentials (E_{An}) and cathode potentials (E_{Cat}) were then corrected based on the solution conductivity and electrode distances from the reference electrode with the following equations [36,40]:

$$\frac{R_\Omega}{l} = \frac{10^3}{\sigma A} \quad (1)$$

$$E_{An} = E_{An,m} - \left(\frac{10^3 R_{\Omega}\, d_{An-RE}}{l}\right) i \quad (2)$$

$$E_{Cat} = (E_{An} + U) + \left(\frac{10^3 R_{\Omega}\, d_{Cat-RE}}{l}\right) i \quad (3)$$

where R_{Ω}/l is the solution ohmic resistance per distance (Ω cm^{-1}), d_{An-Cat} is the distance between anode and cathode (1 cm), σ is the solution conductivity measured for 50 mM PBS (mS cm^{-1}), A is the electrode projected area (cm^2), d_{An-RE} and d_{Cat-RE} are the distances from the anode or cathode to the reference electrode (cm). All potentials are reported versus SHE.

2.3. Electrochemical analysis

The electrode potential slope (EPS) analysis was used to evaluate the area-based resistances and working potentials of the anodes and cathodes [36,41]. Briefly, the linear region of the cathode or anode polarization curves at current densities near the maximum power density (typically 3–9 A m^{-2} in 50 mM PBS) was fitted to $E = ai + b$, where E is the electrode potential (mV), i is the current density (A m^{-2}), a is the slope and b is the y-intercept. The magnitude of the slope a was then the electrode specific resistance ($R_{An,s}$ or $R_{Cat,s}$, mΩ m^2), and the magnitude of the y-intercept was the experimental open circuit half–cell potential ($E_{An,e0}$ or $E_{Cat,e0}$, mV). The calculated electrode specific resistance and experimental open circuit half–cell potential are independent of non–electrode variables such as reactor configuration or media type, providing a valid evaluation of the electrode performance and for cross–study comparison.

Linear sweep voltammetry (LSV) was conducted to evaluate the electrochemical performance of fabricated cathodes in an abiotic electrochemical cell containing two chambers (each 2 cm in length, 3 cm in diameter), with an anion exchange membrane placed in between (AEM; AMI-7001, Membrane International Inc., USA) [42]. A square platinum mesh (1 cm by 2 cm) was used as the counter electrode and the electrolyte was 50 mM PBS prepared as described above. An Ag/AgCl reference electrode was placed close to the cathode and remained in position during LSV tests. A multichannel potentiostat (VMP3 Multichannel Workstation, Biologic Science Instruments, USA) was used to sweep the potentials from +0.509 V to – 0.209 V (vs. SHE) at a scan rate of 0.1 mV s^{-1} for 7 times to ensure steady conditions. The LSV tests were conducted in a constant temperature room (30 °C).

Coulombic efficiencies were calculated for three consecutive cycles at an external resistance of 1000 Ω based on changes in chemical oxygen demand (COD) concentration as previously described [10,43],

$$C_E = \frac{M_s \int_0^{t_b} I dt}{F b_{es} v \Delta C} \quad (4)$$

where M_s is the molecular weight of substrate, ΔC is the change of substrate concentration over the batch cycle over time t_b, F is Faraday's constant, v is the volume of the MFC chamber, and b_{es} is the moles of electrons for the substrate. Both influent and effluent COD were prefiltered with 0.2 μm syringe filter (Millipore, USA) to remove bacteria prior to tests using COD digestion vials (Hach, USA). All tests were conducted in duplicate.

2.4. Surface morphology and characterization

The surface morphology of different cathodes was characterized by scanning electron microscopy (SEM; Nova NanoSEM 630, FEI Company, USA). The cathodes were dried in an oven at 60 °C for 2 h to remove any water or liquid prior to the analysis. The cathode surfaces were sputter coated with 10 nm of iridium to avoid charging effect prior to the SEM imaging. Energy dispersive X-ray spectroscopy (EDS, Silicon Drift Detector-X Max^N, Oxford Instruments, UK) was conducted on the same sample surfaces to examine the elemental distribution of Fe on Fe–N$_4$/AC catalyst surface.

To examine hydrophobicities of the Fe–N$_4$/AC cathodes, contact angle measurements were conducted using an Automated Goniometer/Tensiometer (Model 260, Ramé-hart Instrument Co. USA). A cathode specimen was placed horizontally on a sample stage, and a 5 μL droplet of DI water was dropped on the cathode by a syringe equipped with a 100 μL pipette tip. The images were captured dynamically at 1 s interval and analyzed (DROPimage Advanced software) to obtain the contact angle by a geometrical method (sessile drop).

Water evaporation from MFC reactors equipped with different Fe–N$_4$/AC cathodes, was calculated by quantifying the electrolyte volume of each reactor after one cycle (24 h). The feed solution (28 mL) described above was added into all reactors at the beginning of one cycle. After operation for one cycle, the effluent of each reactor was poured into flasks to calculate the final volume and therefore the water evaporation by difference. To ensure accuracy, all tests were conducted in duplicate and conducted for three consecutive cycles.

3. Results and discussion

3.1. Cathode performance in MFCs and electrochemical cells

The performance of MFCs with Fe–N$_4$/AC cathodes based on power densities increased with the amount of Fe–N$_4$ catalyst added to the cathodes. The highest maximum power density of 2.5 ± 0.1 W m^{-2} was obtained with the MFCs equipped with 10 wt% Fe–N$_4$/AC cathodes, which was 25% higher than that for the MFCs with plain AC cathodes (no Fe–N$_4$ addition) of 2.0 ± 0.01 W m^{-2} (Fig. 1A). A maximum power density of 2.3 ± 0.04 W m^{-2} was obtained for MFCs with 1.0 wt% Fe–N$_4$/AC cathodes, slightly lower than that for 10 wt% Fe–N$_4$/AC cathodes due to less catalyst loading. With an even lower catalyst loading, the 0.1 wt% Fe–N$_4$/AC cathodes produced a maximum power density of 2.0 ± 0.1 W m^{-2}, which was similar to 2.0 ± 0.01 W m^{-2} for plain AC cathodes (Fig. 1A), suggesting that 0.1 wt% Fe–N$_4$/AC was too low to significantly boost the ORR.

The improvement in MFC performance was due to the enhancement in cathode activity based on an EPS analysis. The $E_{Cat,e0}$ (experimental open circuit half-cell potential for cathode) for 10 wt% Fe–N$_4$/AC cathodes was increased to 453 ± 8 mV compared to 360 ± 6 mV for the plain AC cathodes, which was a 26% increase (Fig. 1B). The $E_{Cat,e0}$ for 1.0 wt% Fe–N$_4$/AC cathodes was 426 ± 10 mV, which was also slightly higher than that for AC cathodes due to the addition of Fe–N$_4$ catalyst. A similar $E_{Cat,e0}$ of 374 ± 5 mV was obtained for 0.1 wt% Fe–N$_4$/AC cathodes to that of AC cathodes, which was consistent with the power density test (Fig. 1B). The increased $E_{Cat,e0}$ from the Fe–N$_4$/AC cathodes represented a higher oxygen reduction reactivity compared to plain AC cathodes, which resulted from the Fe–N$_4$ catalyst being more reactive towards oxygen reduction (4 e$^-$ transfer) than the AC catalyst (2 e$^-$ transfer) [23,44,45].

No significant difference in $R_{Cat,s}$ (cathode specific resistance) was observed for AC (25 ± 1 mΩ m^2), 0.1 wt% Fe–N$_4$/AC (27 ± 1 mΩ m^2), 1.0 wt% Fe–N$_4$/AC (29 ± 2 mΩ m^2) and 10 wt% Fe–N$_4$/AC (27 ± 1 mΩ m^2) cathodes (Fig. 1B), due to their similar cathode structure. The anode performance for all MFC reactors remained similar in terms of $E_{An,e0}$ (experimental open circuit half-cell potential for anode, −274 ± 3 mV on average) and $R_{An,s}$ (anode specific resistance, 12 ± 1 mΩ m^2 on average) (Fig. 1C, Table S1), further demonstrating the difference in power production resulted from the different cathode reactivity.

The 10 wt% Fe–N$_4$/AC cathodes also showed much better performance in abiotic LSV tests compared to AC cathode. For example, at a current density of 7 A m^{-2} (near the maximum power density point obtained in polarization tests) the 10 wt% Fe–N$_4$/AC cathodes had a potential of 0.164 V, which was 64% more positive than 0.1 V for AC cathodes proving higher oxygen reduction activity (Fig. 1D). Although the addition of Fe–N$_4$ catalyst on AC has boosted the cathodic

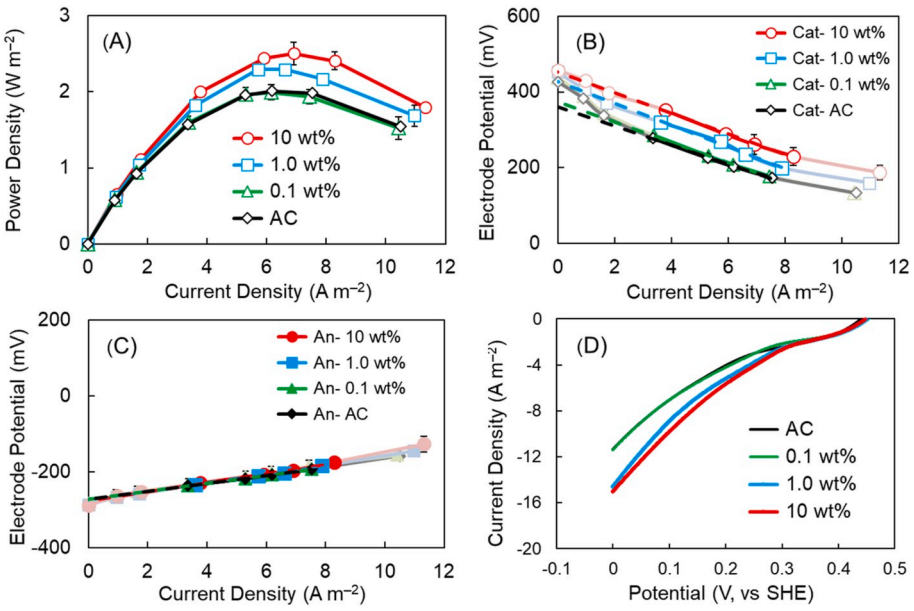

Fig. 1. (A) Power density curves in 50 mM PBS for AC and Fe–N_4/AC (0.1, 1.0 and 10 wt%) cathodes. (B, C) Cathode and anode potentials in 50 mM PBS with corrected solution resistance (The dashed lines represent the data that would be obtained from polarization tests, while the thick solid lines show the linearized portion of the slopes that are used to calculate the anode (R_{An}) and cathode (R_{Cat}) resistances). (D) LSV curves for AC and Fe–N_4/AC (0.1, 1.0 and 10 wt%) cathodes in an electrochemical cell.

performance, the amount of Fe–N_4 addition was limited to 10 wt% as a further increase in added mass led to a loose and fragile catalyst layer that was unsuitable for cathode fabrication, due to the formation of excess Fe–N_4 granular particles on AC surfaces.

3.2. Cathode surface properties

No significant surface morphology change was observed on the cathode surfaces. The AC and all Fe–N_4/AC cathodes remained similarly rough displaying a porous surface structures in SEM images (Fig. 2A–D), with typical distributions of irregular clumps composed of AC/PTFE or Fe–N_4/AC/PTFE mixtures. The Fe–N_4 catalyst was uniformly distributed on the cathode surface based on elemental mapping of Fe with EDS (Fig. 2B–D). For 0.1 wt% Fe–N_4/AC cathode, the Fe atom (brown color) was sparsely distributed on the cathode surface due to the low amount addition of Fe–N_4 catalyst (Fig. 2B). As the weight percentage of Fe–N_4 catalyst increased to 10 wt%, the brown color indicating Fe became darker proving the immobilization of more Fe–N_4 catalyst on cathode surface (Fig. 2D).

The surface hydrophobicity of the Fe–N_4/AC cathodes was greatly

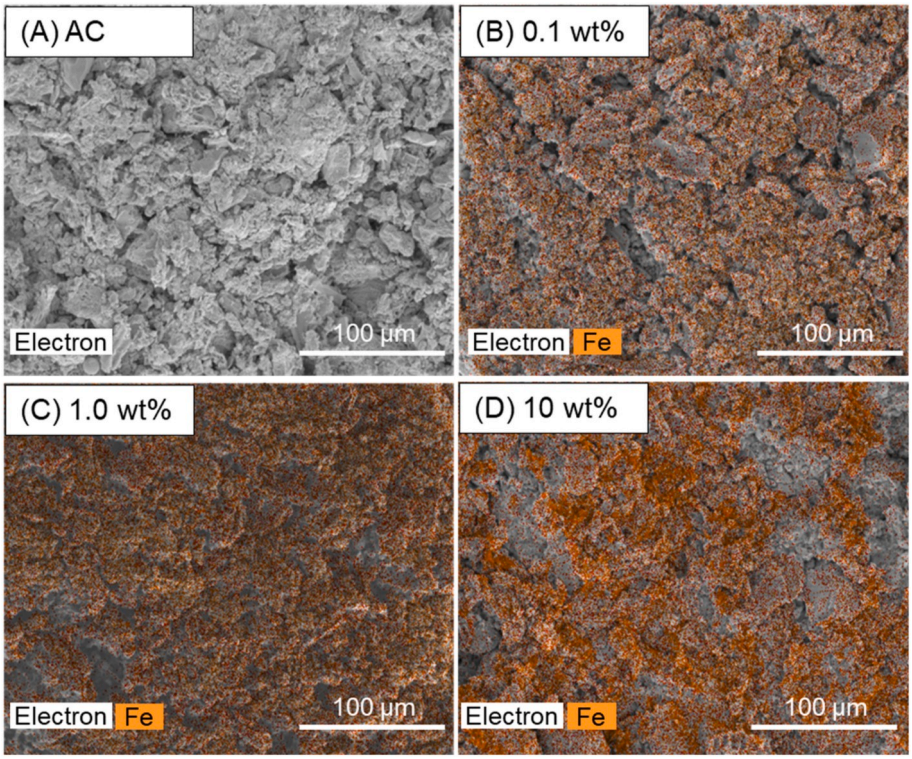

Fig. 2. SEM images with Fe element mapping by EDS for (A) AC, (B) Fe–N_4/AC (0.1 wt%), (C) Fe–N_4/AC (1.0 wt%), (D) Fe–N_4/AC (10 wt%) cathodes (The brown color represents Fe element). (For interpretation of the references to color in this figure legend, the reader is referred to the Web version of this article.)

enhanced bases on dynamic imaging of water droplets on the cathode surfaces. The water droplet was well retained on the surface of the 10 wt % Fe–N_4/AC cathode for the complete 5 s after initial contact with the cathode surface, while the water droplet quickly sank into the plain AC cathode proving the hydrophobicity enhancement due to the addition of the Fe–N_4 catalyst (Fig. 3A and D). The 0.1 and 1.0 wt% cathodes also showed increases of hydrophobicity by retaining the water droplet better than the plain AC (Fig. 3B and C). The incorporation of 10 wt% Fe–N_4 catalyst altered the cathode surface from hydrophilic to be between hydrophobic and superhydrophobic based on contact angle measurements. The static contact angle for 10 wt% Fe–N_4/AC cathodes was 110 ± 4° (after 1 s) (Fig. 4), which was higher than 90° (hydrophobic) but less than 145° (superhydrophobic) [46]. The plain AC cathode was hydrophilic with a static contact angle of 83 ± 5° (Fig. 4). As these cathodes were porous, the water droplet gradually wet the cathodes with subsequently decreased contact angles. However, the contact angle for the 10 wt% Fe–N_4/AC cathodes was well maintained above 90° during the dynamic imaging of 5 s compared to the contact angles for other cathodes, demonstrating the greatly increased hydrophobicity.

Typical AC cathodes are hydrophilic due to the hydrophilic carboxyl or hydroxyl groups of the AC material, so that hydrophobic polymers such as PTFE adopted have been added to increase hydrophobicity [29, 30]. However, only a small amount of such hydrophobic polymers were used to avoid hindering ion transport or blocking catalytic sites, which still made the AC cathode very hydrophilic as observed by water droplet contact angle measurements (Fig. 4). Therefore, immobilizing a hydrophobic catalyst of Fe–N_4 on the AC surface was more effective in boosting the cathode hydrophobicity without lowering the cathode performance.

3.3. Water evaporation, cell voltage and coulombic efficiency

With improved hydrophobicity, the water evaporation through 10 wt% Fe–N_4/AC cathodes was reduced during the MFC operation. The volumes of water evaporated for MFCs were 1.2 ± 0.2 mL for the 10 wt% Fe–N_4/AC cathodes, compared to 2.5 ± 0.1 mL for MFCs with AC cathodes (Fig. 5A). The images of the solutions in the reactors after one cycle operation also clearly showed evidence that water evaporation in the MFCs with 10 wt% Fe–N_4/AC cathode was greatly reduced

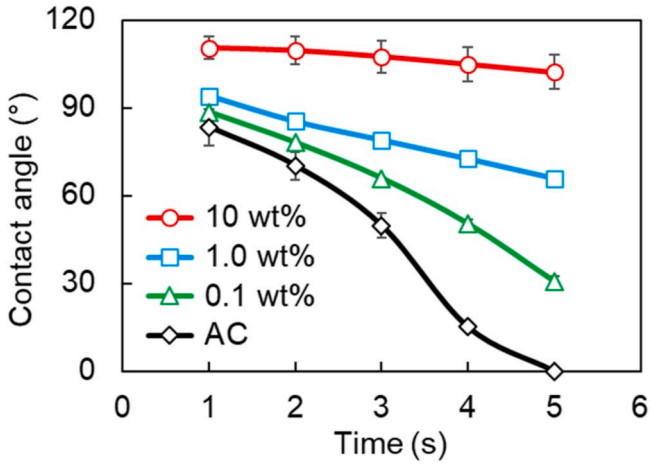

Fig. 4. Dynamic contact angle for AC and Fe–N_4/AC (0.1, 1.0 and 10 wt %) cathodes.

compared to that with plain AC cathode (Figs. S1A and 1D). Less water evaporation was due to hydrophobicity enhancement which hindered water vapor transport, which also reduced oxygen penetration.

The MFCs with 10 wt% Fe–N_4/AC cathodes exhibited both higher voltage and longer voltage duration compared to AC cathodes. The stable voltage generation was 621 ± 0.3 mV for the MFCs with 10 wt% Fe–N_4/AC cathodes (averaged by 10 voltage points in the middle of the cycle), which was higher than 591 ± 0.4 mV for MFCs with AC cathodes for the cycle on day 4 (Fig. 5B). The higher voltage generation with 10 wt% Fe–N_4/AC cathodes was owing to the higher catalytic reactivity of the immobilized Fe–N_4 catalyst. For the cycle on day 4, the MFCs with 10 wt% Fe–N_4/AC cathodes stably produced electricity for 0.9 d before the cell voltage started to decline, which was 50% longer than 0.6 d for MFCs with AC cathodes (Fig. 5B). Similar trends of longer duration of voltage generation were observed in the following two cycles, demonstrating greater electrical output from MFCs using 10 wt% Fe–N_4/AC cathodes.

The coulombic efficiency was also increased for MFCs with 10 wt% Fe–N_4/AC cathodes compared to that with AC cathodes. For 10 wt%

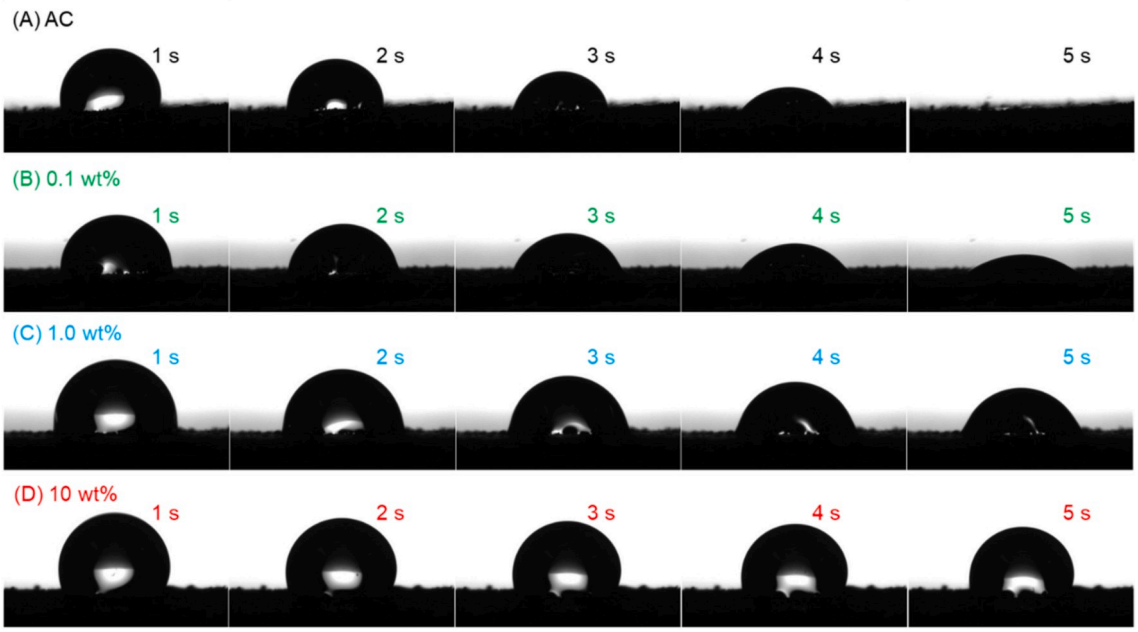

Fig. 3. Dynamic imaging of water droplets on (A) AC, (B) Fe–N_4/AC (0.1 wt%), (C) Fe–N_4/AC (1.0 wt%), (D) Fe–N_4/AC (10 wt%) cathodes with time interval of 1 s.

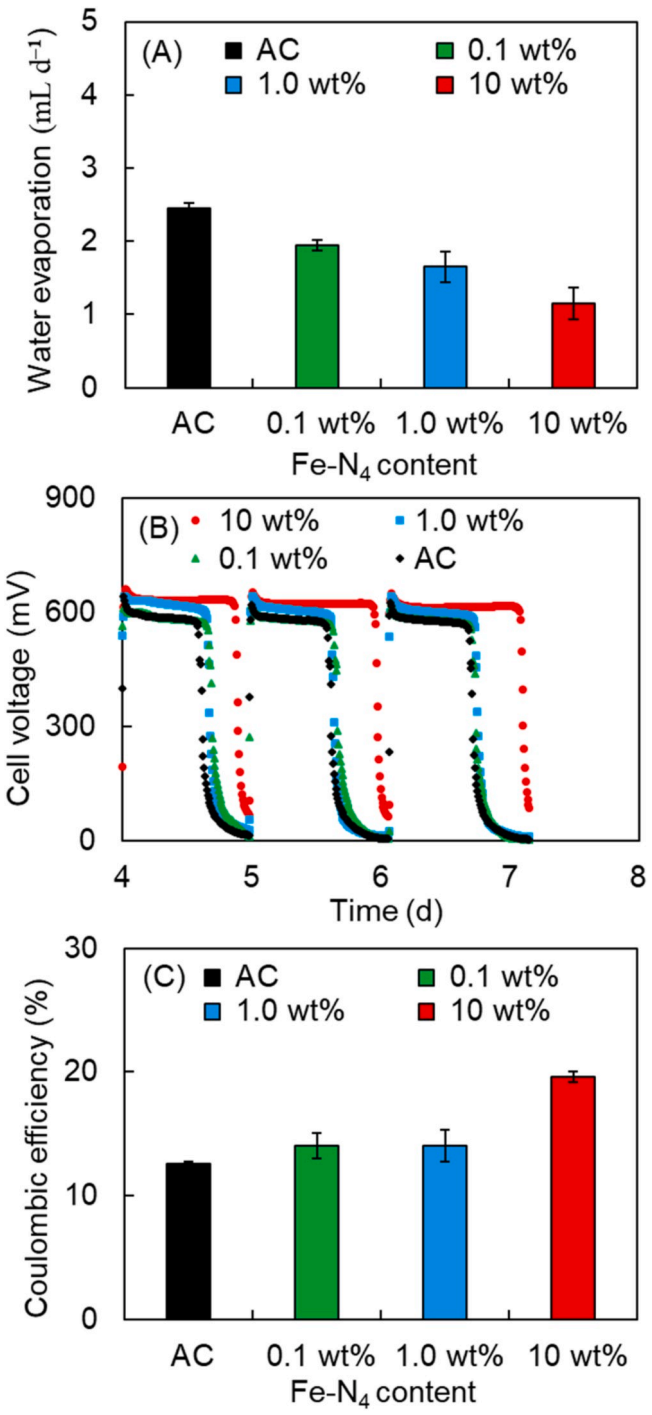

Fig. 5. (A) Water evaporation loss for 1 cycle (1 d) (B) Cell voltage and (C) Coulombic efficiency for MFCs with AC and Fe–N_4/AC (0.1, 1.0 and 10 wt%) cathodes at an external resistance of 1000 Ω.

Fe–N_4/AC cathodes, the coulombic efficiency was 20 ± 0.5%, which was ~54% higher than 13 ± 0.2% for AC cathodes (Fig. 5C). The coulombic efficiencies of the 0.1 and 1.0 wt% Fe–N_4/AC cathodes were not significantly improved probably due to the low amount of Fe–N_4 addition. The improved coulombic efficiency from 10 wt% Fe–N_4/AC cathodes might have resulted from the enhanced hydrophobicity that reduced water loss and avoided too much oxygen penetration into the solution, which could then promote the growth of aerobic bacteria and reduce electricity generation [1,47]. More traditional strategies of improving the coulombic efficiency have been to reduce the oxygen diffusion and water evaporation by adding dense diffusion layers to the air side of the cathode, but this approach usually lowered power production [48]. Therefore, application of this hydrophobic Fe–N_4/AC composite catalyst demonstrated dual advantages of enhancing the coulombic efficiency as well as power density.

4. Conclusions

A hydrophobic Fe–N_4 catalyst was immobilized on AC surfaces to fabricate hydrophobic Fe–N_4/AC air cathodes for MFCs. With an increasing weight percentage of Fe–N_4 catalyst addition, the Fe–N_4/AC cathodes showed increasing cathodic performance relative to the plain AC cathodes, with the best performance from 10 wt% Fe–N_4/AC cathodes. Incorporation of this hydrophobic catalyst endowed the Fe–N_4/AC cathodes good hydrophobicity with less water evaporation and enhanced coulombic efficiency compared to plain AC cathodes. The use of a hydrophobic Fe–N_4 catalyst was therefore an effective and novel approach to simultaneously increase the power density and coulombic efficiency for electricity generation in MFCs. Future studies are still needed for designing other low cost hydrophobic catalysts for practical applications of this approach.

Declaration of competing interestCOI

The authors declare that they have no known competing financial interests or personal relationships that could have appeared to influence the work reported in this paper.

CRediT authorship contribution statement

Wulin Yang: Conceptualization, Data curation, Formal analysis, Methodology. **Xu Wang:** Writing - original draft. **Moon Son:** Writing - original draft. **Bruce E. Logan:** Writing - original draft.

Acknowledgements

This research was supported by Penn State University.

Appendix A. Supplementary data

Supplementary data to this article can be found online at https://doi.org/10.1016/j.jpowsour.2020.228264.

References

[1] B.E. Logan, Microbial Fuel Cells, John Wiley & Sons, Inc., Hoboken, NJ, 2008.
[2] W. Yang, K.-Y. Kim, P.E. Saikaly, B.E. Logan, Energy Environ. Sci. 10 (2017) 1025–1033.
[3] X. Long, H. Wang, C. Wang, X. Cao, X. Li, J. Power Sources 415 (2019) 145–153.
[4] K.-Y. Kim, W. Yang, B.E. Logan, Water Res. 80 (2015) 41–46.
[5] C. Santoro, M. Kodali, N. Shamoon, A. Serov, F. Soavi, I. Merino-Jimenez, I. Gajda, J. Greenman, I. Ieropoulos, P. Atanassov, J. Power Sources 412 (2019) 416–424.
[6] Y. Dong, W. He, D. Liang, C. Li, G. Liu, J. Liu, N. Ren, Y. Feng, J. Power Sources 441 (2019) 227124.
[7] D.R. Lovley, Nat. Rev. Microbiol. 4 (2006) 497–508.
[8] B.E. Logan, P. Aelterman, B. Hamelers, R. Rozendal, U. Schröder, J. Keller, S. Freguiac, W. Verstraete, K. Rabaey, Environ. Sci. Technol. 40 (2006) 5181–5192.
[9] X. Song, J. Liu, Q. Jiang, Y. Qu, W. He, B.E. Logan, Y. Feng, J. Power Sources 395 (2018) 221–227.
[10] W. Yang, F. Zhang, W. He, J. Liu, M.A. Hickner, B.E. Logan, J. Power Sources 269 (2014) 379–384.
[11] X. Tian, M. Zhou, C. Tan, M. Li, L. Liang, K. Li, P. Su, Chem. Eng. J. 348 (2018) 775–785.
[12] S. Rout, S. Parwaiz, A.K. Nayak, J.L. Varanasi, D. Pradhan, D. Das, J. Power Sources 450 (2020) 227679.
[13] Y. Wang, K. Zhong, Z. Huang, L. Chen, Y. Dai, H. Zhang, M. Su, J. Yan, S. Yang, M. Li, J. Power Sources 450 (2020) 227681.
[14] F.S. Farahani, B. Mecheri, M.R. Majidi, M.A.C. de Oliveira, A. D'Epifanio, F. Zurlo, E. Placidi, F. Arciprete, S. Licoccia, J. Power Sources 390 (2018) 45–53.
[15] W. Yang, W. He, F. Zhang, M.A. Hickner, B.E. Logan, Environ. Sci. Technol. Lett. 1 (2014) 416–420.
[16] W. Yang, B.E. Logan, Environ. Sci.: Water Res. Technol. 2 (2016) 858–863.

[17] S. Zhang, W. Su, K. Li, D. Liu, J. Wang, P. Tian, J. Power Sources 396 (2018) 355–362.
[18] Y. Liu, Y.-S. Fan, Z.-M. Liu, Chem. Eng. J. 361 (2019) 416–427.
[19] B. Liang, S. Guo, Y. Zhao, I.U. Khan, X. Zhang, K. Li, C. Lv, J. Power Sources 450 (2020) 227683.
[20] B. Liang, K. Li, Y. Liu, X. Kang, Chem. Eng. J. 358 (2019) 1002–1011.
[21] K. Zhong, M. Li, Y. Yang, H. Zhang, B. Zhang, J. Tang, J. Yan, M. Su, Z. Yang, Appl. Energy 242 (2019) 516–525.
[22] F.-Y. Zheng, R. Li, S. Ge, W.-R. Xu, Y. Zhang, J. Power Sources 446 (2020) 227356.
[23] V.J. Watson, C. Nieto Delgado, B.E. Logan, Environ. Sci. Technol. 47 (2013) 6704–6710.
[24] B. Zhang, Z. Wen, S. Ci, S. Mao, J. Chen, Z. He, ACS Appl. Mater. Interfaces 6 (2014) 7464–7470.
[25] C. Santoro, A. Serov, R. Gokhale, S. Rojas-Carbonell, L. Stariha, J. Gordon, K. Artyushkova, P. Atanassov, Appl. Catal., B 205 (2017) 24–33.
[26] F. Jaouen, V. Goellner, M. Lefevre, J. Herranz, E. Proietti, J.P. Dodelet, Electrochim. Acta 87 (2013) 619–628.
[27] W. Yang, B.E. Logan, ChemSusChem 9 (2016) 2226–2232.
[28] F. Zhang, G. Chen, M.A. Hickner, B.E. Logan, J. Power Sources 218 (2012) 100–105.
[29] H. Dong, H. Yu, X. Wang, Q. Zhou, J. Feng, Water Res. 46 (2012) 5777–5787.
[30] H. Dong, H. Yu, X. Wang, Environ. Sci. Technol. 46 (2012) 13009–13015.
[31] R.J.N. Jasinski, 201 (1964) 1212-1213.
[32] Y. Yuan, B. Zhao, Y. Jeon, S. Zhong, S. Zhou, S. Kim, Biores. Technol. 102 (2011) 5849–5854.
[33] Y. Yuan, J. Ahmed, S. Kim, J. Power Sources 196 (2011) 1103–1106.
[34] C. Santoro, R. Gokhale, B. Mecheri, A. D'Epifanio, S. Licoccia, A. Serov, K. Artyushkova, P.J.C. Atanassov, ChemSusChem 10 (2017) 3243–3251.
[35] B. Mecheri, V.C. Ficca, M.A.C. de Oliveira, A. D'Epifanio, E. Placidi, F. Arciprete, S. Licoccia, Appl. Catal., B 237 (2018) 699–707.
[36] W. Yang, X. Wang, R. Rossi, B.E. Logan, Chem. Eng. J. (2019) 122522.
[37] W. Yang, K.-Y. Kim, B.E. Logan, Biores. Technol. 197 (2015) 318–322.
[38] B.E. Logan, S. Cheng, V. Watson, G. Estadt, Environ. Sci. Technol. 41 (2007) 3341–3346.
[39] S. Cheng, D. Xing, D.F. Call, B.E. Logan, Environ. Sci. Technol. 43 (2009) 3953–3958.
[40] B.E. Logan, E. Zikmund, W. Yang, R. Rossi, K.-Y. Kim, P.E. Saikaly, F. Zhang, Environ. Sci. Technol. 52 (2018) 8977–8985.
[41] R. Rossi, B.P. Cario, C. Santoro, W. Yang, P.E. Saikaly, B.E. Logan, Environ. Sci. Technol. 53 (2019) 3977–3986.
[42] W. Yang, V.J. Watson, B.E. Logan, Environ. Sci. Technol. 50 (2016) 8904–8909.
[43] F. Rezaei, T.L. Richard, B.E. Logan, J. Power Sources 192 (2009) 304–309.
[44] G. Dong, M. Huang, L. Guan, Phys. Chem. Chem. Phys. 14 (2012) 2557–2559.
[45] T. Li, Y. Peng, K. Li, R. Zhang, L. Zheng, D. Xia, X. Zuo, J. Power Sources 293 (2015) 511–518.
[46] K.-Y. Law, J. Phys. Chem. 5 (2014) 686–688.
[47] Y. Fan, H. Hu, H. Liu, J. Power Sources 171 (2007) 348–354.
[48] S. Cheng, H. Liu, B.E. Logan, Electrochem. Commun. 8 (2006) 489–494.